



# Ragweed pollen production and dispersion modelling within a regional climate system, calibration and application over Europe

Li Liu<sup>1,2</sup>, Fabien Solmon<sup>1</sup>, Robert Vautard<sup>3</sup>, Lynda Hamaoui-Laguel<sup>3,4</sup>, Csaba Zsolt Torma<sup>1</sup>, and Filippo Giorgi<sup>1</sup>

<sup>1</sup>Earth System Physics Section, the Abdus Salam International Centre for Theoretical Physics, Trieste, Italy

<sup>2</sup>Guizhou Key Laboratory of Mountainous Climate and Resources, Guiyang, China

<sup>3</sup>Laboratoire des Sciences du Climat et de l'Environnement, IPSL, CEA-CNRS-UVSQ, UMR8212, Gif sur Yvette, France

<sup>4</sup>Institut National de l'Environnement Industriel et des Risques, Parc technologique ALATA, Verneuil en Halatte, France

Correspondence to: Li Liu (liliulish@outlook.com) and Fabien Solmon (fsolmon@ictp.it)

Received: 27 August 2015 – Published in Biogeosciences Discuss.: 3 November 2015

Revised: 17 April 2016 – Accepted: 21 April 2016 – Published: 11 May 2016

**Abstract.** Common ragweed (*Ambrosia artemisiifolia* L.) is a highly allergenic and invasive plant in Europe. Its pollen can be transported over large distances and has been recognized as a significant cause of hay fever and asthma (D'Amato et al., 2007; Burbach et al., 2009). To simulate production and dispersion of common ragweed pollen, we implement a pollen emission and transport module in the Regional Climate Model (RegCM) version 4 using the framework of the Community Land Model (CLM) version 4.5. In this online approach pollen emissions are calculated based on the modelling of plant distribution, pollen production, species-specific phenology, flowering probability, and flux response to meteorological conditions. A pollen tracer model is used to describe pollen advective transport, turbulent mixing, dry and wet deposition.

The model is then applied and evaluated on a European domain for the period 2000–2010. To reduce the large uncertainties notably due to the lack of information on ragweed density distribution, a calibration based on airborne pollen observations is used. Accordingly a cross validation is conducted and shows reasonable error and sensitivity of the calibration. Resulting simulations show that the model captures the gross features of the pollen concentrations found in Europe, and reproduce reasonably both the spatial and temporal patterns of flowering season and associated pollen concentrations measured over Europe. The model can explain 68.6, 39.2, and 34.3 % of the observed variance in starting, central, and ending dates of the pollen season with associated root mean square error (RMSE) equal to 4.7, 3.9, and 7.0 days, respectively. The correlation between simulated and

observed daily concentrations time series reaches 0.69. Statistical scores show that the model performs better over the central Europe source region where pollen loads are larger and the model is better constrained.

From these simulations health risks associated to common ragweed pollen spread are evaluated through calculation of exposure time above health-relevant threshold levels. The total risk area with concentration above 5 grains m<sup>-3</sup> takes up 29.5 % of domain. The longest exposure time occurs on Pannonian Plain, where the number of days per year with the daily concentration above 20 grains m<sup>-3</sup> exceeds 30.

## 1 Introduction

*Ambrosia artemisiifolia* L. (common ragweed, hereafter ragweed), is an alien plant that has invaded parts of Europe over the last century, creating severe allergies in populations (Chauvel et al., 2006; Kazinczi et al., 2008; Gallinza et al., 2010; Pinke et al., 2011). It has been shown that concentrations of ragweed pollen down to 5–10 grains m<sup>-3</sup> can lead to health problems for sensitive persons (Tamarcaz et al., 2005). In Europe, ragweed typically flowers from July to October (Kazinczi et al., 2008). Ragweed has developed wind pollination strategy, which allows each plant to produce millions of pollen grains with a diameter of 18–22 µm and containing small air chambers (Payne, 1963). Pollen grains can readily become airborne when conditions are favourable (Dahl et al., 1999; Tamarcaz et al., 2005; Cecchi et al.,

2006; Stach et al., 2007; Smith et al., 2008; Šikoparija et al., 2013).

One of the goals of the project “Atopic diseases in changing climate, land use and air quality” (ATOPICA) (<http://www.atopica.eu>) is to better understand and quantify the effects of environmental changes on ragweed pollen and associated health impacts over Europe. In this context the present study introduces a modelling framework designed to simulate production and dispersion of ragweed pollen. Ultimately these models can be used for investigating the effects of changing climate and land use on ragweed (Hamaoui-Laguel et al., 2015) and for providing relevant data to health impact investigators.

Presently a number of regional models, mostly designed for air quality prevision, incorporate release and dispersion dynamics of pollen (Helbig et al., 2004; Sofiev et al., 2006, 2013; Skjøth, 2009; Efstathiou et al., 2011; Zink et al., 2012; Prank et al., 2013; Zhang et al., 2014). Methods for producing ragweed pollen emission suitable for input to regional scale models have been developed in recent studies (Skjøth et al., 2010; Šikoparija et al., 2012; Chapman et al., 2014). Due to a lack of statistical information related to plant location and amount within a given geographical area, the bottom up approach to produce plant presence inventories is unpractical for most herbaceous allergenic species like ragweed. Quantitative habitat maps for such species are often derived from spatial variations in annual pollen sum, knowledge on plant ecology and detailed land cover information by top-down approach (such as Skjøth et al., 2010, 2013; Thibaudon et al., 2014; Karrer et al., 2015). Lately, an observation-based habitat map of ragweed has been published in the context of the ENV.B2/ETU/2010/0037 project “Assessing and controlling the spread and the effects of common ragweed in Europe” (Bullock et al., 2012). This inventory is further calibrated against airborne pollen observations to reproduce the ragweed distribution with high accuracy, according to Prank et al. (2013). Recently Hamaoui-Laguel et al. (2015) used the observations collected in Bullock et al. (2012), combined with simplified assumptions on plant density and a calibration using observations to obtain a ragweed density inventory map. This approach made use of the Organising Carbon and Hydrology in Dynamic Ecosystems (ORCHIDEE) and the Phenological Modeling Platform (PMP) for obtaining daily available pollens (potential emissions) in Europe.

On average, one ragweed plant can produce  $1.19 \pm 0.14$  billion pollen grains in a year (Fumanal et al., 2007), but resources available (solar radiation, water, CO<sub>2</sub>, and nutrients) for an individual plant during the growth season could alter its fitness and further influence its pollen production (Rogers et al., 2006; Simard and Benoit, 2011, 2012). Fumanal et al. (2007) investigate the individual pollen production of different common ragweed populations in natural environment and propose a quantitative relationship between annual pollen production and plant biomass at the beginning of flowering. This allows to integrate the response of pro-

ductivity to various environmental conditions through land surface model.

The timing of the emission can be estimated from a combination of phenological models and the species specific pollen release pattern driven by short-term meteorological conditions (Martin et al., 2010; Smith et al., 2013; Zink et al., 2013). Ragweed is a summer annual, short-day plant. Before seeds are able to germinate, it requires a period of chilling to break the dormant state (Willemsen, 1975). The following growth and phenological development depends on both temperature and photoperiod (Allard, 1945; Deen et al., 1998a). Flowering is initiated by a shortening length of day but could be terminated by frost (Dahl et al., 1999; Smith et al., 2013) or drought (Storkey et al., 2014). A number of phenological models have been developed for ragweed, either based on correlation fitting between climate and phenological stages (García-Mozo et al., 2009) or explicitly represented by biological mechanisms (Deen et al., 1998a; Shrestha et al., 1999; Storkey et al., 2014; Chapman et al., 2014). The mechanistic models take into account the responses of development rates to temperature, photoperiod, soil moisture, or stress condition (frost, drought, etc.). Mostly they are based on growth experiments but have to enforce a standard calendar date or a fixed day length for the onset of flowering when they are used in real conditions. While the airborne pollen observations from European pollen monitoring sites have a high year to year, site to site variability. Therefore it might be practical to combine the mechanistic model with correlation fitting when the knowledge of plant physiology and local adaptation of phenology are not sufficiently known at the moment.

In this paper, we present a pollen emission scheme that incorporate plant distribution, pollen production, species-specific phenology, flowering probability distribution, and pollen release based on recent studies. By combining the emission scheme with a transport mechanism a pollen simulation framework within the Regional Climate Model (RegCM) version 4 is then developed to study ragweed pollen dispersion behaviours on a regional scale. In Sect. 2 we provide a description of the RegCM-pollen simulation configuration, emission parameterization details, the processing of plant spatial density and observations data used for calibration in the study. In Sect. 3 we define the model experiment, explain the method used to calibrate ragweed density, present the simulation results of pollen season, evaluate the performances of the coupled model system over a recent period covered with observations, and finally present the climatological information about the ragweed pollen risk over European domain on a decadal timescale. Summary and conclusions appear in Sect. 4.

## 2 Materials and methods

The development of RegCM-pollen model is based on the Abdus Salam International Centre for Theoretical Physics

(ICTP) regional climate model, i.e. RegCM4, which has been used for a number of years in a wide variety of applications (Giorgi et al., 2006, 2012; Meleux et al., 2007; Pal et al., 2007). In this framework, we develop a pollen model for ragweed which calculates (i) the seasonal production of pollen grains and (ii) their emission and atmospheric processes (transport and deposition) determining regional pollen concentrations. As detailed hereafter pollen emission and transport are developed in the preexisting framework of the RegCM atmospheric chemistry module (Solmon et al., 2006, 2012; Zakey et al., 2006; Tummon et al., 2010; Shalaby et al., 2012). Pollen production is developed in the framework of the Community Land Model (CLM) version 4.5 (Oleson et al., 2013), which is the land surface scheme coupled to RegCM. Figure 1 gives an overview of such development framework. In the following subsections, we give details about the important data and steps of the development.

## 2.1 Observed pollen concentrations

Pollen observations are central for calibration and validation of the pollen module as discussed further. The pollen data are provided by the European Aeroallergen Network (<https://ean.polleninfo.eu/Ean/>) and affiliated national aerobiology monitoring network RNSA (France, <http://www.pollens.fr/en/>), ARPA-Veneto (Italy, <http://www.arpa.veneto.it>), and Croatian organizations including the Institute of Public Health, the Department of Environmental Protection and Health Ecology at Institute of Public Health “Andrija Štampar” and Associate-degree college of Velika Gorica. The archives cover ragweed pollen concentrations (expressed as  $\text{grain m}^{-3}$ ) with daily resolution from 44 observations stations from 2000–2012 year (Table 1). The pollen observation sites range from 42.649 to 48.300° N and from 0.164 to 21.583° E. The sites are grouped for study purposes into four regions: France (FR), Italy (IT), Germany–Switzerland (DE+CH) and central Europe (Central EU) including Austria, Croatia, and Hungary (Fig. 2). Ragweed pollens are collected at an airflow rate of  $10 \text{ L min}^{-1}$  using volumetric spore traps based on the Hirst (1952) design. Samples were examined with light microscopy for the identification and counting of pollen grains. The International Association for Aerobiology (IAA) recommends for the samples reading at magnification  $400\times$  minimum of 3 longitudinal bands or at least 12 transverse bands or minimum 500 random fields (Jäger et al., 1995). The actual sampling methods (longitudinal, transverse or random) and magnifications may vary between the several national networks but are generally compliant (Jato et al., 2006; Skjøth et al., 2010; García-Mozo et al., 2009; Sofiev et al., 2015; Galán et al., 2014; Thibaudon et al., 2014). We based our study on daily pollen concentrations, although for some stations hourly data are available. The observations period ranges from 2000 to 2012 but for some stations observations only cover part of this period. The observations of 2000–2010 are designed for model application and evalua-

tion about ragweed pollen risk. The data for 2011 and 2012 are left and only used for verifying pollen season simulated by a phenology model.

## 2.2 Model setup

Ragweed pollen simulations are carried out for a European domain ranging from approximately 35 to 70° N, and from 20° W to 40° E (Fig. 2). The horizontal resolution is 50 km, with 23 atmospheric layers from the surface to 50 hPa. Initial and lateral atmospheric boundary conditions are provided by ERA-Interim analysis at 1.5° spatial resolution and 6 h temporal resolution. Weekly SSTs are obtained from the NOAA optimum interpolation (OI) SST analysis (with weekly ERA sea surface temperatures). Beside CLM4.5 as a land surface scheme, other important physical options are Holtslag PBL scheme (Holtslag et al., 1990) for boundary layer, Grell scheme (Grell, 1993) over land and Emanuel scheme (Emanuel and Zivkovic-Rothman, 1999) over ocean for convective precipitation, the SUBEX scheme (Pal et al., 2000) for large-scale precipitation. Aerosol and humidity are advected using a semi-Lagrangian scheme. The period 2000–2010 is chosen for the study. Even though the focus of the study is July–October of flowering season, the model is integrated continuously throughout the year notably for simulating ragweed phenology. To compare with the observation described in Sect. 2.1, simulated pollen concentrations time series are interpolated to the station locations and averaged daily.

## 2.3 Ragweed spatial density

Ragweed spatial distribution is obtained through a procedure discussed in Hamaoui-Laguel et al. (2015). For country where observations are available and of sufficient quality, ragweed distribution is assumed to result from habitat suitability combined with infestation (not all suitable habitats are populated). The habitat suitability is assumed to scale as the product of the fraction of suitable land use surface  $H(x, y)$  with a climate suitability index  $CI(x, y)$  calculated from the SIRIUS ecological model (Storkey et al., 2014). The infestation rate is derived from density of  $10 \times 10 \text{ km cells } K(x, y)$  with plant presence as reported in Bullock et al. (2012). Assuming a homogeneous surface distribution of suitable habitats within each model grid cell ( $50 \times 50 \text{ km}$ ) and assuming that observers only investigate suitable areas, the probability of plant presence (or infestation rate) should then be proportional to  $K(x, y)/25$ . But considering that an observer probably finds ragweed plants more often than what a random search would predict, the density should actually be lower than that predicted by  $K(x, y)/25$ . We assumed that infestation rate actually scales as  $(K(x, y)/25)^r$ , with  $r > 1$ , taken here equals to 2. The final ragweed density  $D_p$  (in  $\text{plant m}^{-2}$ ) at 50 km resolution is therefore obtained from the infestation rate, surface fraction of suitable land use, and climatic suit-

**Table 1.** General information (2000–2010) for pollen observation sites. The annual pollen sum is calculated from 15 July to 31 October. Only years with data available exceeding 67 % between 20 July and 2 September are used to determine the observed start date and years with data available exceeding 56 % between 3 September and 18 October are used to determine the end date.

Station	city	Country	Longitude	Latitude	Source	Years available (n)	Annual pollen sum (grains m <sup>-3</sup> )	Observed pollen season (Julian day)			Simulated pollen season (Julian day)			RMSEs of pollen season		
								start	centre	end	start	centre	end	start	centre	end
ATPULL	Oberpull	AT	16.504	47.503	EAN	6	656.0	224	243	268	226	242	264	3.6	8.2	0.0
ATWIEN	Vienna	AT	16.35	48.300	EAN	11	1607.7	227	247	276	230	248	276	7.1	4.3	7.6
CHGENE	Geneva	CH	6.15	46.19	EAN	11	200.0	230	243	264	231	243	270	5.2	2.7	10.0
CHLAUS	Lausanne	CH	6.64	46.52	EAN	11	96.2	231	238	255	232	238	265	5.8	4.1	5.9
DEFREI	Freiburg	DE	7.866	48.00	EAN	11	24.9	239	240	248	236	237	246	2.0	3.0	7.9
AIX	Aix-en-P	FR	5.442	43.535	RNSA	11	238.8	232	243	260	232	245	258	0.0	0.0	0.7
FRANGO	Angoulême	FR	0.164	45.649	RNSA	4	191.5	234	244	256	234	244	255	6.0	3.4	3.4
FRANNE	Amnevy	FR	6.133	45.904	RNSA	6	81.3	226	231	247	227	234	256	0.0	0.0	0.0
FRAVIG	Avignon	FR	4.805	43.92	RNSA	6	361.7	230	242	261	230	242	261	5.5	4.1	6.6
FRBESA	Besançon	FR	6.026	47.241	RNSA	6	53.8	239	242	245	244	247	251	0.0	0.0	0.0
FRBOUB	Bourg en B	FR	5.221	46.21	RNSA	5	593.6	229	241	258	229	240	258	5.1	4.2	5.2
FRBOUR	Bourges	FR	2.396	47.084	RNSA	2	300.0	221	236	263	227	238	267	10.0	0.7	0.7
FRCHAL	Chalon S S	FR	4.845	46.78	RNSA	6	252.6	229	241	256	229	240	257	2.7	3.7	4.1
FRCLER	Clermont-F	FR	3.094	45.759	RNSA	6	251.8	236	244	256	235	243	256	5.8	2.8	5.6
FRDJIO	Dijon	FR	5.066	47.319	RNSA	6	134.7	236	246	255	238	247	257	7.9	1.2	6.1
LYON	Lyon	FR	4.825	46.344	RNSA	11	1528.1	222	240	264	224	242	266	4.0	5.3	5.1
FRMONT	Montluçon	FR	2.606	46.344	RNSA	6	197.4	235	243	257	234	242	256	5.9	3.1	4.9
FRNEVE	Nevers	FR	3.161	46.987	RNSA	6	834.2	225	242	261	226	241	261	2.7	1.9	6.6
FRNIME	Nîmes	FR	4.35	43.833	RNSA	6	157.3	236	245	258	236	244	258	2.2	3.3	6.4
FRORLE	Orléans	FR	1.898	47.908	RNSA	3	21.3	236	245	258	236	244	258	2.2	3.3	6.4
ROUSSILLON	Roussillon	FR	4.812	45.371	RNSA	9	5210.2	221	242	262	223	242	263	3.3	3.1	8.0
TOULON	Toulon	FR	5.978	43.127	RNSA	11	133.6	238	246	251	238	243	254	2.5	2.0	0.0
ERTOUS	Toulouse	FR	1.454	43.559	RNSA	6	56.2	245	248	256	243	245	254	0.0	0.0	0.0
FRVICH	Vichy	FR	3.434	46.131	RNSA	3	343.0	227	240	259	229	240	261	6.1	2.8	3.7
BELOVAR	Bjelovar	HR	16.843	45.897	HRTEAM	6	6993.8	221	240	261	222	239	262	2.9	2.5	4.1
DUBROVNIK	Dubrovnik	HR	18.076	42.649	HRTEAM	6	152.8	240	242	257	241	243	265	3.4	2.9	4.3
KARLOVAC	Karlovac	HR	15.542	45.492	HRTEAM	3	5159.0	218	237	256	219	238	260	1.9	1.4	3.8
OSIJEK	Osijek	HR	18.688	45.558	HRTEAM	4	6924.5	218	240	259	219	241	261	3.3	1.7	4.7
SLAVONSKI	Slavonski	HR	18.023	45.154	HRTEAM	3	13964.0	220	240	266	223	242	267	4.2	3.1	8.0
SPLIT	Split	HR	16.299	43.54	HRTEAM	3	281.3	232	249	259	233	254	266	0.7	8.6	5.5
ZADAR	Zadar	HR	15.235	44.107	HRTEAM	4	515.2	232	244	270	234	245	275	3.4	4.1	9.7
HRZAGR	Zagreb	HR	16.00	45.800	EAN	8	4207.5	221	240	262	222	240	263	4.3	1.8	4.5
HUDEBR	Debreceen	HU	21.583	47.533	EAN	11	7275.4	217	240	264	220	240	265	5.0	3.0	8.5
HUGYOR	Győr	HU	17.600	47.667	EAN	11	2976.5	222	241	268	223	242	271	3.3	5.3	9.4
AGORDO	Ağordo	IT	12.021	46.284	ARPA-Veneto	3	0.3	222	241	268	223	242	271	3.3	5.3	9.4
BELLUNO	Belluno	IT	12.200	46.136	ARPA-Veneto	5	1.4	235	244	262	236	243	264	2.0	2.7	9.8
JESOLO	Jesolo	IT	12.661	45.51	ARPA-Veneto	5	221.6	235	244	262	236	243	264	2.0	2.7	9.8
LEGNAGO	Legnago	IT	11.315	45.185	ARPA-Veneto	5	175.7	231	244	255	231	245	256	1.9	6.2	11.8
ITMAGE	Magenta	IT	8.883	45.466	EAN	4	5584.8	221	242	267	223	244	263	4.0	4.7	6.6
MESTRE	Meestre	IT	12.25	45.48	ARPA-Veneto	5	290.5	234	244	263	234	243	263	5.2	3.4	10.2
ITPARM	Parma	IT	10.31	44.800	EAN	7	244.1	226	240	257	227	240	258	5.7	2.4	6.2
ROVIGO	Rovigo	IT	11.786	45.049	ARPA-Veneto	4	81.0	240	244	250	238	244	250	6.0	3.0	3.5
VERONA	Verona	IT	10.992	45.427	ARPA-Veneto	5	172.4	230	242	255	230	244	257	1.6	6.7	8.3
VICENZA	Vicenza	IT	11.562	45.546	ARPA-Veneto	5	223.1	232	244	260	232	245	262	7.2	4.9	10.8



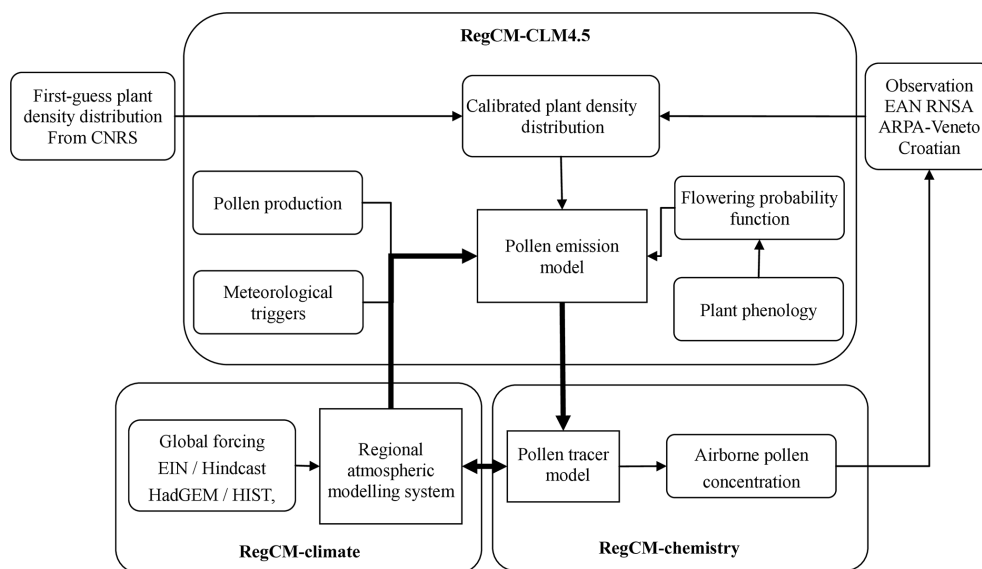


Figure 1. Ragweed pollen modelling within online RegCM-pollen simulation framework.

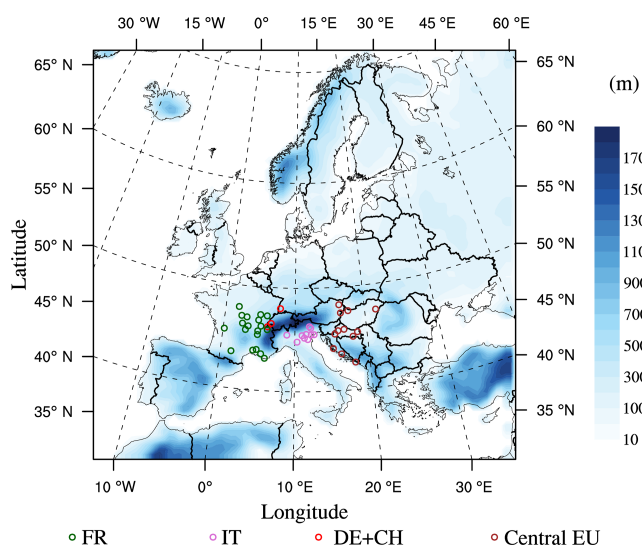


Figure 2. Model domain and the observation sites with topography.

ability index as

$$D_p(x, y) = \text{const} \cdot H(x, y) \cdot CI(x, y) \cdot \left(\frac{K(x, y)}{25}\right)^r \quad (1)$$

Here  $\text{const} = 0.02$  is assumed to be the maximal density ( $\text{plant m}^{-2}$ ) in the most suitable habitats (Efstathiou et al., 2011),  $H(x, y)$  taken as the crop and urban lands in CMIP5 land use classification (Hurtt et al., 2006). For countries with low-quality observations or with no available inventories, the detection probability is replaced by the average over neighbouring countries with reliable data.

## 2.4 Parameterization of the pollen emission flux

Pollen emission patterns on regional scale depend on plant density, production, and meteorological conditions. The parameterization of pollen emission flux is a modified version of Helbig et al. (2004). The vertical flux of pollen particles  $F_p$  in a given grid cell is assumed to be proportional to the product of a characteristic pollen grain concentration per plant individual  $c^*$  ( $\text{grain m}^{-3} \text{ plant}^{-1}$ ) and the local friction velocity  $u_*$ . This potential flux is then modulated by a plant-specific factor  $c_e$  that describes the likelihood of blossoming, and a meteorological adjustment factor. Finally the flux is scaled up at the grid level using the plant density  $D_p$  ( $\text{plant m}^{-2}$ ) discussed previously in Sect. 2.3.

$$F_p = D_p \cdot c_e \cdot K_e \cdot c^* \cdot u_*, \quad (2)$$

## 2.5 Pollen production

The characteristic concentration  $c^*$  is related to pollen grain production using

$$c^* = \frac{q_p}{\text{LAI} \cdot H_s}, \quad (3)$$

where  $q_p$  is the annual pollen production in grains per individual plant ( $\text{grains plant}^{-1}$ ),  $\text{LAI} = 3$  is the leaf area index term, and  $H_s = 1$  is the canopy height (m). These later parameter are determined on the basis of CLM4.5 C3 grass land use categories during summer.

Annual pollen production  $q_p$  is estimated from plant biomass production, based on an assumption that pollen production per plant is a function of the plant dry biomass, i.e. the accumulated net primary production (NPP) of CLM4.5 C3 grass plant functional type during the growth season.

Based on this assumption,  $q_p$  is calculated following Fumanal et al. (2007) (Eq. 4). This parameterization integrates the response of pollen grain productivity to various environmental conditions affecting C3 grass NPP, including climate variables and atmospheric CO<sub>2</sub> concentration for example. It involves a variety of biophysical and biogeochemical processes at the surface such as photosynthesis, phenology, allocation of carbon/nitrogen assimilates in the different components of plant, biomass turnover, litter decomposition, and soil carbon/nitrogen dynamics.

$$\log_{10}(q_p) = 7.22 + 1.12\log_{10}(\text{plant dry biomass}) \quad (4)$$

In this approach, yearly total pollen production calculation from mature plant dry biomass needs to be determined in advance, i.e. before integration of the pollen modelling chain. This is done by making a preliminary RegCM-CLM4.5 run with prognostic NPP activated and archived. Alternatively, in order to reduce simulation costs and insure model portability to other domains we also built a precomputed global C3 grass yearly accumulated NPP data base. This data can be directly interpolated and prescribed to RegCM4 for pollen runs. This global data base is built by running the land component CLM4.5 of the Community Earth System Model version 1.2 (CESM1.2) (Oleson et al., 2013) with the Biome-BGC biogeochemical model (Thornton et al., 2002, 2007) enabled and forced by CRUNCEP (Viovy, 2011). We acknowledge that NPP obtained this way is not fully consistent with RegCM simulated climate but this approach represents a reasonable and practical compromise.

## 2.6 Flowering probability density distribution

In Eq. (2),  $C_e$  is a probability density function accounting for the likelihood of the plant to flower and effectively release pollen in the atmosphere. The inflorescences of common ragweed consist of many individual flowers that reach anthesis sequentially (Payne, 1963). At the beginning of the season only a few plants flower and the amount of available pollen grains is small, regardless of the favourable meteorological conditions. The number of flowers increases with time until a maximum is reached. Afterwards, the number decreases again until the end of the pollen season. To represent this dynamic, we use the normal distribution function reported in Prank et al. (2013). The probability distribution of flowering time is represented by a Gaussian depending on “accumulated biological days” BD, and centred midway between flowering starting and ending biological days  $BD_{fe}$  and  $BD_{fs}$ :

$$c_e = \text{const} \cdot \frac{1}{\sigma\sqrt{2\pi}} \cdot e^{-\frac{(\text{BD} - \frac{BD_{fe} + BD_{fs}}{2})^2}{2\sigma^2}}, \quad (5)$$

where  $\text{const} = 20 \times 10^{-4}$  is determined by adjusting the integrated amount of pollens between  $BD_{fe}$  and  $BD_{fs}$  to the total yearly production  $q_p$  determined from NPP.  $\sigma$  is the standard deviation determined by the length of the season, considering

that the season represents about 4 standard deviations of the Gaussian distribution  $4\sigma = BD_{fe} - BD_{fs}$ . The probability distribution is however set to zero as soon as the daily minimum temperature is below 0°, considering that first frost set up the end of ragweed activity (Dahl et al., 1999). In the following section we describe how biological days (BD) are effectively determined.

## 2.7 Phenology representation and flowering season definition

### 2.7.1 Biological days

For simulating the timing of the flowering season, we adapt the mechanistic phenology model of Chapman et al. (2014), which is based on growth experiments (Deen et al., 1998a, b, 2001; Shrestha et al., 1999). Phenology is simulated using BD accumulated for the current year of simulation and from the first day ( $t_0$ ) after the spring equinox for which daily minimum temperature exceeds a certain threshold  $T_{\min}$  defined further (Chapman et al., 2014). BD on time  $t$  depends on key environmental variables through:

$$\text{BD}(T, L, \theta) = \int_{t_0} r_T(T) \cdot r_L(L) \cdot r_S(\theta) \cdot dt, \quad (6)$$

where  $r_T$ ,  $r_L$ ,  $r_S$  are the response of development rates to temperature  $T$ , photoperiod  $L$ , and soil moisture  $\theta$ , respectively. In this approach, biological day varies according to local climate as illustrated in Sect. 3.2. The phenological development of ragweed before flowering is separated into vegetative and reproductive phases controlled by different factors. Vegetative development stages are germination to seedling emergence (4.5 BD) and emergence to end of juvenile phase (7.0 BD) (Deen et al., 2001). The development rate at the germination to seedling emergence is assumed to be affected by temperature and soil moisture, while the rate at the emergence to end of juvenile phase is affected by temperature alone. From the end of the juvenile phase to the beginning of anthesis (13.5 BD) (Deen et al., 2001) the reproductive development phase takes place and is affected by temperature and photoperiod. Vegetative and reproductive processes are assumed to have an identical response to temperature based on the cardinal temperature determined by Chapman et al. (2014).

$$r_T(T) = \begin{cases} 0 & T < T_{\min} \\ \left( \frac{T - T_{\min}}{T_{\text{opt}} - T_{\min}} \left( \frac{T_{\max} - T}{T_{\max} - T_{\text{opt}}} \right)^{\frac{T_{\max} - T_{\text{opt}}}{T_{\text{opt}} - T_{\min}}} \right)^c & T_{\min} \leq T \leq T_{\max} \\ 0 & T > T_{\max} \end{cases}, \quad (7)$$

where  $T_{\min}$ ,  $T_{\text{opt}}$ ,  $T_{\max}$  are minimum, optimum, and maximum growing temperatures with values 4.88, 30.65, 42.92° respectively.  $c$  is a scaling parameter with value of 1.696. All

these parameters are derived from growth trial data (Deen et al., 1998a, b, 2001; Shrestha et al., 1999).

The response of development rates to photoperiod is simulated using a modified version of function presented by Chapman et al. (2014)

$$r_L(L) = \begin{cases} e^{(L-14.0)\ln(1-L_s)} & L \geq 14.0 \\ 1 & L < 14.0 \end{cases} \quad (8)$$

where  $L$  is day length, expressed in hours. The photoperiod response delays plant development when the day is longer than the threshold photoperiod fixed to 14.0 h (Deen et al., 1998b).  $L_s$  is a photoperiod sensitivity parameter varying between 0 and 1, which controls development delay and can be adjusted according to sensitivity test to reflect ragweed phenology adapted to local ecological environment. Photoperiods are assumed to affect reproductive development from the end of the juvenile phase.

The response of development rates to soil moisture is assumed to occur from the germination to seedling emergence stage. We use a linear function similar to the one used to account for soil moisture impact on biogenic emission activity factor in MEGAN (Guenther et al., 2012)

$$r_S(\theta) = \begin{cases} 0 & \theta < \theta_w \\ \frac{\theta - \theta_w}{\theta_{opt} - \theta_w} & \theta_w \leq \theta \leq \theta_1 \\ 1 & \theta > \theta_1 \end{cases} \quad (9)$$

where  $\theta$  is volumetric water content ( $\text{m}^3 \text{m}^{-3}$ ),  $\theta_w$  ( $\text{m}^3 \text{m}^{-3}$ ) is wilting point (the soil moisture level below which plants cannot extract water from soil) and  $\theta_{opt}$  ( $= \theta_w + 0.1, \text{m}^3 \text{m}^{-3}$ ) is the optimum soil moisture level in the seed zone over which the development rate reaches maximum (Deen et al., 2001).

According to this phenology model, a total of about 25 BD are theoretically needed to reach the beginning of pollen season  $\text{BD}_{fs}$  from the initiation date of BD accumulation. However this model relies on parameters determined from controlled conditions and transposition to natural environment is not straightforward in order to calculate a realistic  $\text{BD}_{fs}$ . Moreover, the model does not allow to calculate a priori the end of season date  $\text{BD}_{fe}$  required in Eq. (5). While we do rely on BD to represent the phenological evolution within the season, we however constrain the starting and ending biological days of the season ( $\text{BD}_{fs}$  and  $\text{BD}_{fe}$ ) based on observations, as explained hereafter.

### 2.7.2 Dates of the flowering season

Experimentally, pollen season can be defined in a number of ways from observed pollen concentrations and listed for example in Jato et al. (2006). A widely used definition is the period during which a given percentage of the yearly pollen sum is reached. Another definition refers to the period between the first and last day with pollen concentrations ex-

ceeding a specific level. Looking at the temporal distribution of observations, particularly long distribution tails can be found in some cases at the beginning and the end of the pollen season, especially in stations where pollen levels are moderate. This makes the definition of pollen season rather imprecise, while it is in general more constrained in areas with high yearly pollen sum. In our approach, we define the start of the pollen season from 44 observation stations (described in Sect. 2.1) as the following: the first day of a series of 3 days in a weekly window for which the pollen concentrations exceed  $5 \text{ grains m}^{-3}$ , and after 2.5 % of the yearly pollen sum has been reached. The end of the pollen season is defined as the following: the last day of a series of 3 days in a weekly window for which the pollen concentrations exceed  $5 \text{ grains m}^{-3}$ , just before reaching 97.5 % of the yearly pollen sum. ( $5 \text{ grains m}^{-3}$  is supposed the minimum threshold to induce medically relevant risks.) The centre of the pollen season is simply defined as the time when the yearly pollen sum reaches 50 %. Kriging method is then used to spatially interpolate pollen season dates determined for each station over the simulation domain. For each grid cell,  $\text{BD}_{fs}$  and  $\text{BD}_{fm}$  are determined by simulating and accumulating biological days up to the experimentally defined starting and mid-season dates. Ending season dates is calculated as  $2\text{BD}_{fm} - \text{BD}_{fs}$  according Eq. (5). This methodology requires again a pre-calculation run of RegCM4/CLM4.5 where simulated BD is output in order to be matched with observed season dates for each year. Once this step is achieved, spatially resolved  $\text{BD}_{fs}$  and  $\text{BD}_{fe}$  can be obtained by averaging across the years and used to perform the integrated pollen run.

### 2.8 Instantaneous release factor

In Eq. (2), the  $K_e$  factor accounts for short-term modulation of pollen flux from meteorological conditions. Following Sofiev et al. (2013)  $K_e$  is a function of wind speed, relative humidity, and precipitation calculated by RegCM-CLM45 during the run.

$$K_e = \left( \frac{h_{\max} - h}{h_{\max} - h_{\min}} \right) \cdot \left[ f_{\max} - \exp\left(-\frac{U + w_*}{U_{\text{sat}}}\right) \right] \cdot \left( \frac{p_{\max} - p}{p_{\max} - p_{\min}} \right) \quad (10)$$

In this formula,  $h$  and  $p$  are relative humidity (%) and precipitation ( $\text{mm h}^{-1}$ ), which do not affect the release until lower thresholds ( $h_{\min}$ ,  $p_{\min}$ ) are reached. After reaching upper thresholds ( $h_{\max}$ ,  $p_{\max}$ ) the pollen release is totally inhibited.  $U$  is the interactive 10 m wind speed ( $\text{m s}^{-1}$ ) connected to RegCM prognostic wind and surface roughness,  $w_*$  is a convective velocity scale ( $\text{m s}^{-1}$ ),  $U_{\text{sat}}$  is the saturation wind speed ( $\text{m s}^{-1}$ ), and  $f_{\max}$  is the maximum value that wind can contribute to the release rate. The definitions of threshold parameters are discussed in detail in Sofiev et al. (2013).

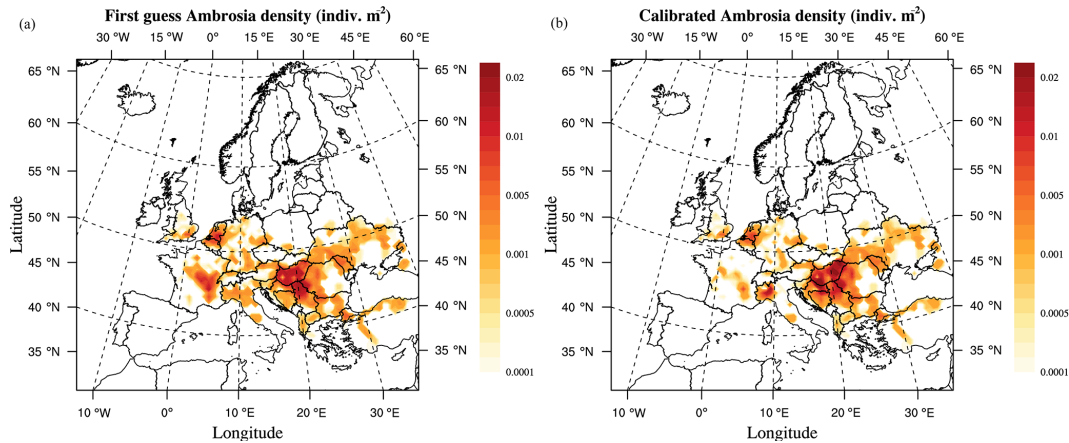


**Figure 3.** First guess (a) and calibrated (b) ragweed density distribution.

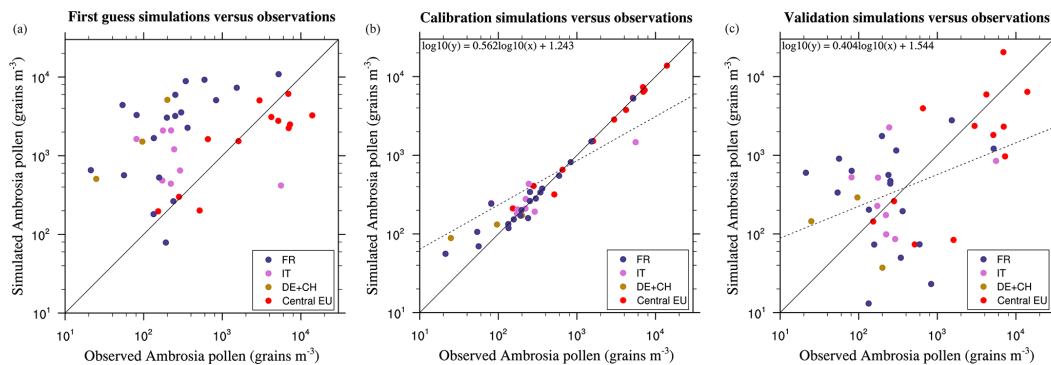


**Figure 4.** Average (2000–2010) annual pollen sum for first guess (a), calibration (b) and validation (c) simulations on sites.

### 3 Model application and evaluation

#### 3.1 First guess simulation and calibration of the ragweed density

A first pollen run is performed using the first guess ragweed density described in Sect. 2 and displayed in Fig. 3a. First guess density map shows maxima of ragweed in the south-east of France, Benelux countries, and central Europe regions. When comparing the resulting field to observation, simulated concentrations obtained with the first guess distribution are generally overestimated over France, Switzerland and Germany, underestimated in parts of central Europe, and have comparable order of magnitude over some Italian and Croatian stations (Fig. 4a). These important biases are in large part due to assumptions made in the construction of the first guess plant density distribution. In order to reduce these biases we perform a model calibration by introducing a correction to the first guess ragweed distribution. For each station, calibration coefficients are obtained by minimizing the yearly root mean square error (RMSE) after constraining the decadal (2000–2010) mean simulated pollen concentration to match the decadal mean observed concentrations

(2000–2010) within an admissible value. Calibration coefficients obtained over each station are then interpolated spatially on the domain using ordinary Kriging technique. Then a calibrated simulation using the calibrated density distribution is carried out and repeated several times. After three iterations, the correlation of yearly totals across observation stations increase from 0.23 to 0.98 and the patterns are clustering around the 1 : 1 line (Fig. 4b).

The final calibrated ragweed distribution (Fig. 3b) shows high density in central Europe including Hungary, Serbia, Bosnia and Herzegovina, Croatia, and western Romania, northern Italy, western France, and also in the southern Netherlands and northern Belgium. The calibration adjusts the density over all the grid cells with ragweed presence by a factor ranging between 0.1 and 4.4 with an average of 0.98.

To estimate the error and sensitivity of this calibration method to the individual stations we implement a five-fold cross validation. The 44 sites are randomly divided into 5 groups. Five calibration experiments are conducted each time with one group left and used for validation respectively. The results of five validation groups are then combined to assess the final performance. With this approach a model measurements Pearson correlation of 0.54 is obtained together with a

normalized root mean squared error of 21 % (Fig. 4c). Without surprise, this is less than when using the full data sets for calibration. In particular a few stations with particularly high concentrations protruding from surrounding sites (for example, ITMAGE and ROUSSILLON) have a large impact on the results of validation. We compared our cross validation (eight or nine sites left out each time) with three papers about ragweed pollen source estimation over the Pannonian Plain, France and Austria (Skjøth et al., 2010; Thibaudon et al., 2014; Karrer et al., 2015). Their cross validations (one site left out each time) show corresponding correlations of 0.37, 0.25, 0.63 and root mean squared error of 25, 16 and 3 %, respectively. Our results are within this range. We agree that caution should be taken in areas without a decent number of station coverage where the calibration cannot be done.

Note that through correction, other systematic sources of errors possibly affecting the modelling chain might also be implicitly corrected, leading to undesirable error compensations. However, after running additional tests (not shown here), for example varying model dynamical boundary conditions, a relatively small impact on pollen model performance is found when compared to the ragweed density distribution impact.

### 3.2 Simulation of pollen season

The simulated starting dates, central dates, and ending dates of pollen season are averaged from 2000 to 2010 and presented in Fig. 5. The pollen season generally shows a positive gradient from the south to the north and from low altitude to high altitude, resulting from the combined effects of temperature, day length, and soil moisture. The starting date varies between 21 July and 8 September. Flowering starts in the central European source regions earlier than in west and north of source regions. The central dates are reached between 1 August and 27 September, without noticeable difference between central and west source regions. Flowering ends in the central later than in the west of source regions. The pollen season is longest in the central main source regions.

Table 2 lists the statistical correlation between simulated and observed pollen starting, central, and ending dates. The model can reproduce starting and central dates better than ending dates. Goodness-of-fit tests show that the models account for 68.6, 39.2, and 34.3 % of the observed variance in starting, central, and ending dates. The RMSE is 4.7, 3.9, and 7.0 days for the pollen starting, central, and ending dates, respectively. The model reproduces the pollen season in the main source regions fairly well (Table 1), where the averaged differences between the simulated and observed pollen season progression are less or equal to 3 days and RMSE is lower than 6 days. For the areas with lower ragweed infestation the results vary widely. The starting dates and central dates are still reproduced well for a majority of the stations while the ending dates are more problematic with averaged

**Table 2.** Statistical correlation between simulated and observed ragweed pollen season for fitting 2000–2010 and prediction (2011, 2012).

period	Explained variance (%)			RMSE		
	start	centre	end	start	centre	end
2000–2010	68.6	39.2	34.3	4.7	3.9	7.0
2011	38.5	0.03	14.4	6.2	5.0	8.0
2012	28.7	48.0	26.1	6.3	3.4	8.2

differences above 6–10 days and RMSE over 8–12 days at some stations. This might result from patchy local ragweed distribution and the effect of long-range transport of pollen, which contributes to the determination of pollen season dates and are assumed to be representative of local flowering in our approach. Some stations also stop pollen measurement before the actual end of pollen season which leads to a lower accuracy of season ending date.

This phenology model is further tested for years of 2011–2012 and compared to observations (Table 2). Despite lower correlations, starting dates in both years and ending dates in 2012 are predicted reasonably well with 38.5, 28.7, and 26.1 % of the explained variance. The model however fails in predicting central dates in 2012 with low correlations to experimentally determined dates. Even so the prediction errors of RMSE for all dates in both years are well controlled and the differences between fitting and prediction RMSE are kept within 1.6 days, which means degradation of model performance has limited effects on the prediction of pollen season. Extending the fitting to several years of observation may contribute to improve the stability and robustness of the fitted threshold and further improve the phenology modellings of ragweed.

### 3.3 Model performance and evaluation

The evaluation of the model performance is made by comparing the modelled to observed airborne pollen concentrations over the 2000–2010 period. In the Taylor diagram on Fig. 6, we present an overview on how the models perform in terms of spatio-temporal correlations, standard deviations, and RMSEs compared to observations. The statistics are given for different timescales of variability: daily, annual, or for the full 11-year period (in this case, it is equivalent to spatial statistics only). Different variables are analysed: the daily concentrations, the annual concentration sums, means, and maxima, and the 11-year concentration sum, mean, and maxima. To plot all the statistics on a single diagram, standard deviation and RMSE are normalized by the standard deviation of observations at the relevant spatiotemporal frequency: observations are thus represented by point OBS on the diagram (perfect correlation coefficient, RMSE = 0 and normalized standard deviation = 1). The closer a point to the

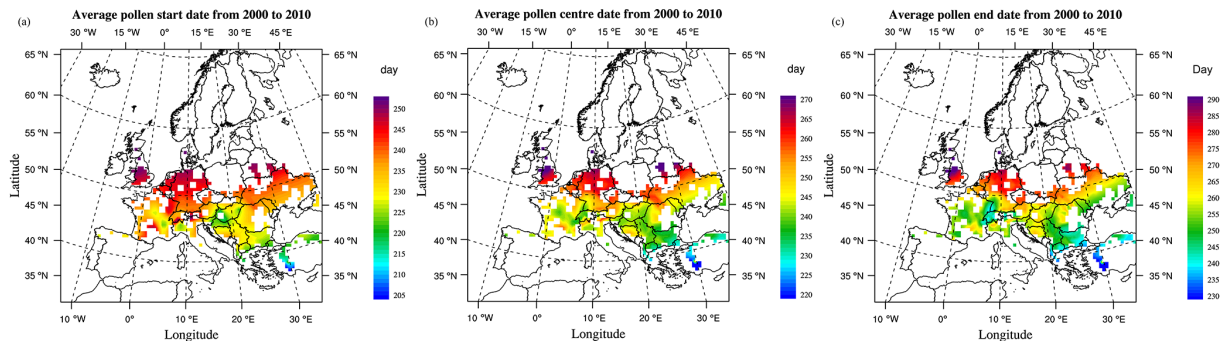


**Figure 5.** Average pollen season (day of the year) from 2000–2010: start dates (a), central date (b), and end dates (c).

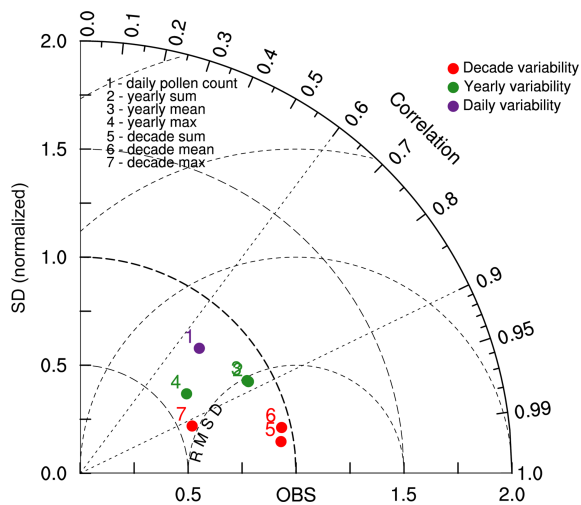


**Figure 6.** Normalized Taylor diagram showing spatial and temporal correlations coefficients, standard deviations and RMSEs between simulations and observations for the period 2000–2010. Standard deviation and RMSE are normalized by the standard deviation of observations at the relevant spatiotemporal frequency.

reference OBS, the best is the model skill for this particular variable.

From the diagram, we can see that the model tends to perform very well when the variability is purely spatial and concentrations averages over the 11-year period (dots 5, 6 are very close to OBS). Not surprisingly it means the uncertainties are reduced to a large extent by the calibration procedure. However, the calibrated simulations do not capture the concentration maximum as well and tend to underestimate the measured spatial standard deviation (decade maximum dot 7 and also for the annual maximum dot 4). The model does not perform that well, but still shows some realism when the variability is involved in both spatial and temporal correlations. The yearly statistics, which reflect the interannual variation of pollen concentrations over the stations, are captured well with correlation coefficients all above 0.80 and normalized standard deviations of 0.89, 0.88, and 0.61 for concentration

sum, mean, and maximum respectively. When scores are calculated for daily concentrations over all the stations, the overall spatial-temporal correlation coefficient reaches 0.69 for a relative standard deviation of 0.80.

Daily variability is obviously the most difficult to simulate but is at the same time the most relevant in terms of pollen health impact. To investigate this point further, the model performance is regionally evaluated with both discrete and categorical statistical indicators as listed in Zhang et al. (2012). The discrete indicators considered in this study include correlation coefficient, normalized mean bias factors (NMBF), normalized mean error factors (NMEF), mean fractional bias (MFB), and mean fractional error (MFE). NMBF  $\leq \pm 0.25$  and NMEF  $\leq 0.35$  are proposed by Yu et al. (2006) as a criteria of good model performance. Boylan and Russell (2006) recommended MFB  $\leq \pm 0.30$  and MFE  $\leq \pm 0.50$  as good performance and MFB  $\leq \pm 0.60$  and MFE  $\leq \pm 0.75$  as acceptable performance for particulate matter pollution. All metrics are computed over daily time series at each station and on a whole European domain (Table 3). For the whole domain, the average values of NMBF, NMEF, MFB, and MFE are  $-0.11$ ,  $0.83$ ,  $-0.15$ , and  $-0.31$ , respectively. Except for NMEF, the indices fall in the range of good performance according to the above criteria. The pollen concentrations over the whole domain are underestimated by a factor of 1.11 based on NMBF. As a measure of absolute gross error, NMEF characterize the spread of the deviation between simulations and observations. Although a relatively large gross error of 0.83 exists, the NMEF obtained here is consistent with what is expected from operational air quality models (Yu et al., 2006; Zhang et al., 2006).

The spatial distributions of correlation coefficient, NMBF, NMEF are shown in Fig. 7. The correlations between simulated and observed daily time series are above 0.6–0.7 in the central Europe source region and are mostly above 0.5–0.6 in the source regions of northern Italy and eastern France, while the correlations are low in areas without strong local emission where the majority of observed pollen may originate from long-range transport or sporadic ragweed sources. Overall 56.8 % of the stations show an NMBF within  $\pm 0.25$



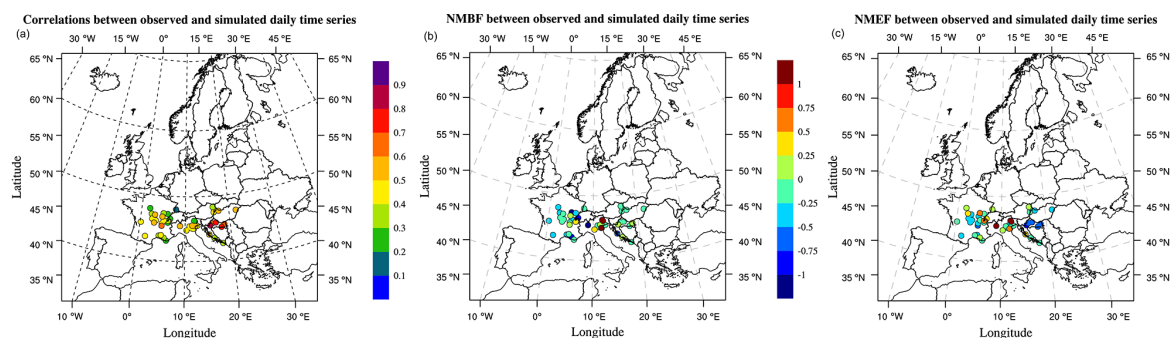


**Figure 7.** Statistical measures between simulated and observed daily pollen time series for each site: correlation coefficients (a), normalized mean bias factors (b) and normalized mean error factors (c).

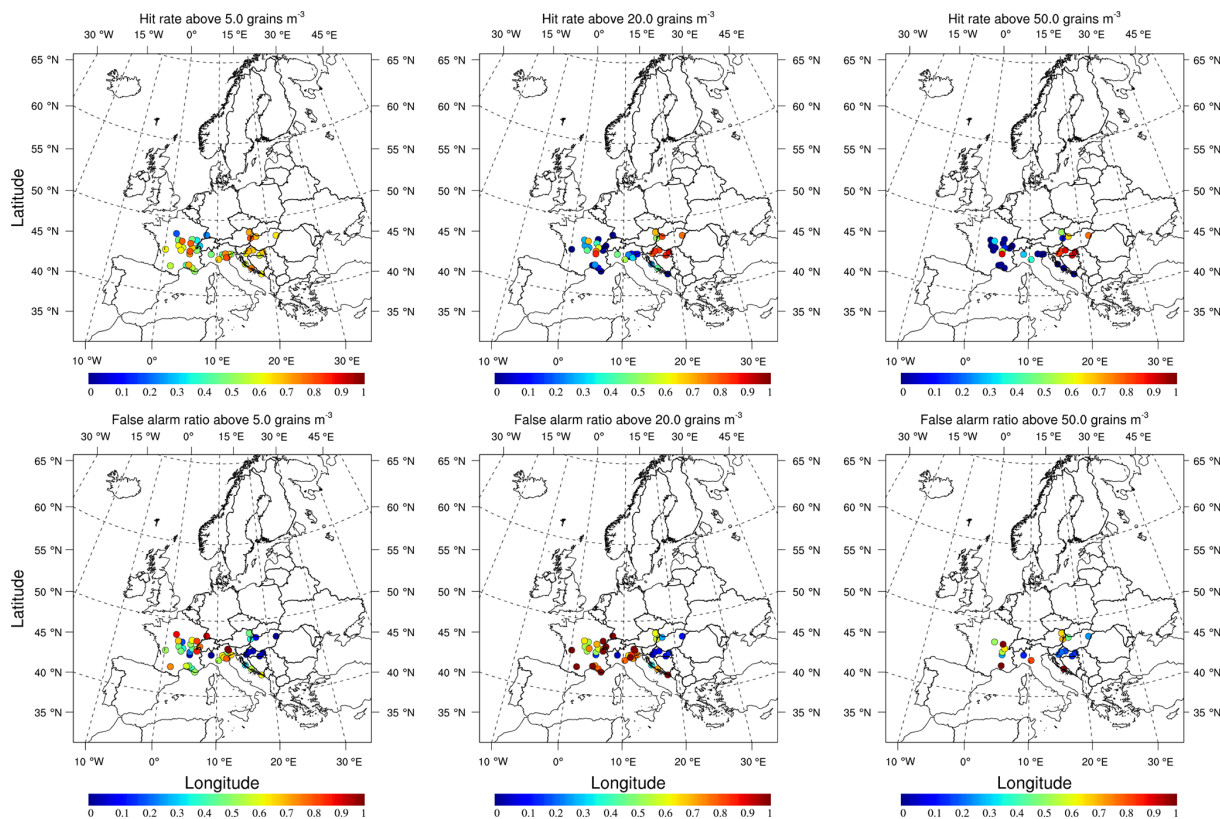


**Figure 8.** Categorical statistics at thresholds of 5 (left column), 20 (middle column), and 50 grains  $\text{m}^{-3}$  (right column): upper panel – hit rate (percentage of correctly predicted exceedances to all actual exceedances), lower panel – false alarm ratio (percentage of incorrectly predicted exceedances to all predicted exceedances).

and 79.5 % are within  $\pm 0.50$ . In the source regions of central Europe and eastern France, almost all NMBF values lie within  $\pm 0.25$ . In northern Italy the model mostly overestimates the mean daily pollen concentrations by factors ranging from 1.25 to above 2.0 (except for ITMAGE station). Simultaneous overestimation and underestimation can be found for neighbouring stations, which reflects probably the influence of local and patchy sources difficult to account for at 50 km resolution. Better performances are ob-

tained for central European source regions, where the majority of NMEF are within 1.0. Performance degrades in France, where most NMEF values are within 1.2. Simulations are more problematic over northern Italy, where values of NMEF are often above 1.2. Generally 51.4 % of the stations with NMEF are within 1.0 and 79.5 % are within 1.4.

A categorical evaluation is done by classifying the values of pollen concentration with regard to the thresholds of 5, 20, and 50 grains  $\text{m}^{-3}$ . Hit rates (fraction of correctly simulated

**Table 3.** Model performance on simulation of daily average concentrations for 2000–2010.

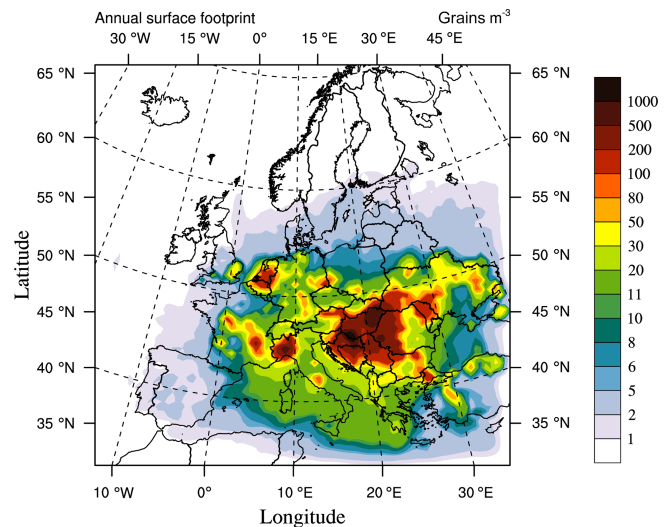
Discrete statistical indicators			
normalized mean bias factors (NMBF)	−0.11		
normalized mean error factors (NMEF)	0.83		
mean fractional bias (MFB)	−0.15		
mean fractional error (MFE)	−0.31		
correlation coefficient ( <i>R</i> )	0.69		
categorical statistical indicators (%)	Threshold (grains m <sup>−3</sup> )		
	5	20	50
Hit rates	67.9	73.3	74.3
false alarm ratio	33.3	31.9	32.2

exceedances out of all observed exceedances) and false alarm ratio (fraction of incorrectly simulated exceedances out of all simulated exceedances) are calculated from daily time series over the period. On the whole domain, hit rates for these thresholds are 67.9, 73.3, and 74.3 % and false alarm ratios are 33.3, 31.9, and 32.2 %, respectively. The model tends to perform better for high threshold exceedance while giving more false alarms for the lower threshold. As shown in Fig. 8, there are however large regional differences in model performance. Over central European source region, correct prediction often exceed 80 % at moderate and high thresholds and false alarms are about 10 % at low and moderate thresholds and 20 % at high threshold. Performance degrades in France and northern Italy source regions, where correct predictions are mostly around 50–70 % at low and moderate thresholds but false alarms are generally high, especially at moderate threshold.

### 3.4 Ragweed pollen distribution pattern and risk assessments

With a reasonable confidence in model results, risks region can be identified over the domain. Risk is defined from certain health-relevant concentration thresholds. First we can consider minimum ragweed concentrations triggering an allergic reaction. These thresholds are based on experiments involving short exposure time to pollen and then extrapolated in order to define health thresholds in terms of daily average concentrations. It is not known, whether a short-time exposure to a large pollen concentration is equivalent to the same dose when less pollen is inhaled over a longer period. Furthermore, these thresholds vary largely between different regions and ethnic groups. The likely range of such daily thresholds is 5–20 grains m<sup>−3</sup> per day estimated by Oswald and Marshall (2008). Very sensitive people can be affected by as few as 1–2 pollen grains m<sup>−3</sup> per day (Bullock et al., 2012).

On this basis, simulated surface concentrations are post-processed to produce 24 h average concentrations. The foot-

**Figure 9.** Annual footprint of ragweed pollen at the surface, obtained by selecting the maximum from daily averaged concentrations during the whole pollen season.

prints of ragweed pollen risk are then obtained by selecting the yearly and monthly maximum from daily averaged concentrations. The yearly and monthly maximums are averaged over the decade (2000–2010) to produce footprints depicted in Figs. 9, 10). The risk is divided into 16 levels to reflect the range of health relevant threshold used in different countries and regions as listed in Table 4.3 of Bullock et al. (2012). The numbers of grid cells at different threshold risk levels are given in Table 4. Hereafter we select some of the representative risk levels to be discussed in more detail. From annual footprint of ragweed pollen spread risk, the area with concentration  $\geq 1$  grains m<sup>−3</sup> occupies almost 50.3 % area of domain, with an average concentration of 23.7 grains m<sup>−3</sup>. The risk pattern extends from European mainland to the seas due to the long-range transport. The lowest risk areas with concentration of 1–5 grains m<sup>−3</sup> are located over the sea as well as in the countries upwind and far from the known sources, such as Spain, UK, Poland, Belarus, and Latvia. The low risk areas with concentration of 5–20 grains m<sup>−3</sup> are found on the periphery of the source regions and over Mediterranean Sea, occupying 18.2 % of domain. The intermediate risk areas with concentration of 20–50 grains m<sup>−3</sup> are close to the sources, taking up 6.1 % of domain. The areas with very strong stress  $\geq 50$  grains m<sup>−3</sup> are concentrated on main sources, taking up 5.2 % of domain.

Temporally, the pollen risk is determined by seasonal evolution (Fig. 10). August is in general the month contributing the most to the annual risk footprint, with an average concentration of 25.6 grains m<sup>−3</sup> (from grid cells with concentration above 1 grains m<sup>−3</sup>). However for some northern regions like Belgium and Germany, the maximum risk is found for September (Fig. 10). Overall September shows important levels 18.9 grains m<sup>−3</sup> when October and July exhibits much



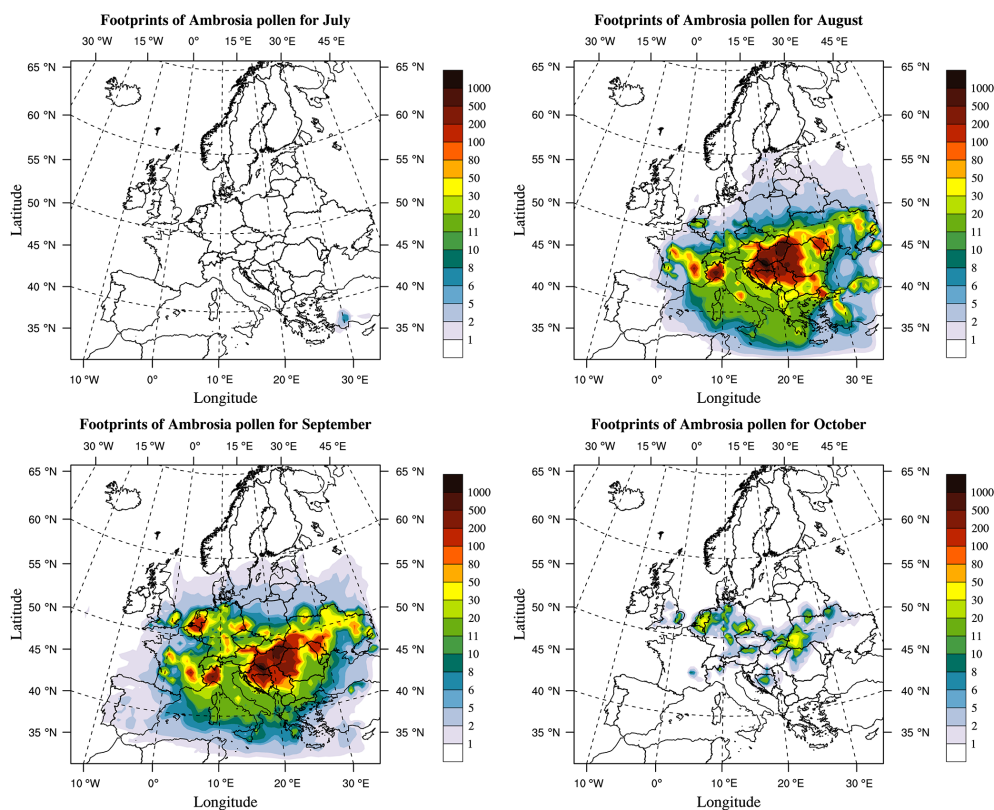


**Figure 10.** Footprints of ragweed pollen at the surface in each month during pollen season, average from 2000–2010, obtained by selecting the maximum from daily averaged concentrations in each month.

**Table 4.** Percent area with the surface concentration of ragweed pollen at different risk levels, average for 2000–2010.

level	Lower bound of the thresholds/ (grain m <sup>-3</sup> )	Percent area in domain				
		Jul	Aug	Sep	Oct	annual
1	0	99.6	61.1	54.3	92.4	49.7
2	1	0.2	6.8	11.5	2.3	9.1
3	2	0.1	8.8	10.2	2.7	11.7
4	5	0.0	2.5	1.9	0.3	2.1
5	6	0.1	3.1	3.6	0.5	3.8
6	8	0.0	2.1	2.7	0.3	2.9
7	10	0.0	1.0	1.2	0.1	1.3
8	11	0.0	6.8	6.5	0.8	8.1
9	20	0.0	2.6	2.1	0.4	3.5
10	30	0.0	1.3	1.9	0.2	2.6
11	50	0.0	1.2	1.3	0.0	1.6
12	80	0.0	0.4	0.4	0.0	0.6
13	100	0.0	1.1	1.4	0.0	1.4
14	200	0.0	1.0	0.8	0.0	1.2
15	500	0.0	0.2	0.2	0.0	0.3
16	1000	0.0	0.0	0.0	0.0	0.1

weaker concentrations. The risk areas associated to pollen for each month are given in Table 4.

Besides the triggering of allergic reactions at a certain threshold, the time of exposure above a certain threshold might also be important, e.g. in terms of sensitization to ragweed pollen. To assess a risk based on this criterion, exposure time, expressed as the decadal average of the number of days per season above a certain threshold, is calculated and reported in Fig. 11. Relevant thresholds are 5, 10, 20, 50 grain m<sup>-3</sup>.

The longest exposure times occurs in Pannonian Plain at all thresholds, reaching for example about 30 days above 20 grains m<sup>-3</sup>. Northern Italy and France can also show some important exposure times. Over the measurement stations, we can compare measured and simulated exposure time at different thresholds as reported in Fig. 11, where measurements are indicated with circles coloured by the measured number of days (left half) and corresponding simulated number of days (right half). Simulated and measured risk agrees reasonably for most stations with in general better comparison for moderate thresholds (10 and 20 grain m<sup>-3</sup>) relative to high or low thresholds. Nevertheless except for a few stations the simulated exposure time tends to be overestimated.

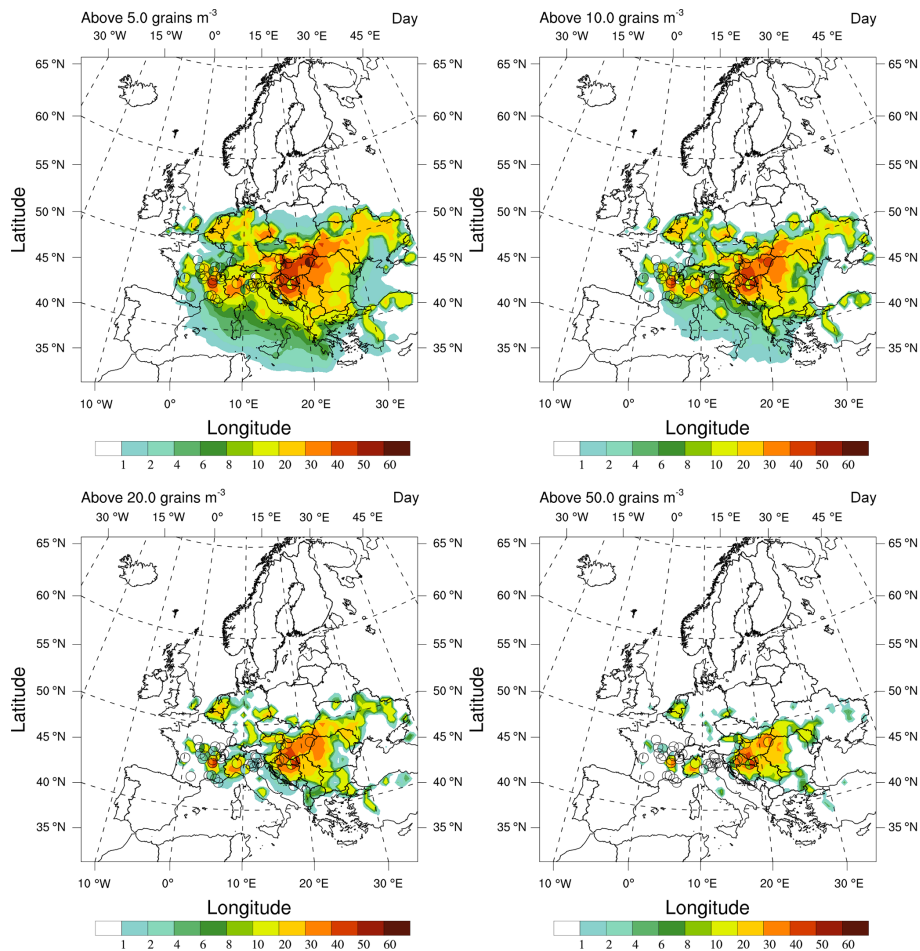


**Figure 11.** Number of days when the daily average concentration exceeding certain risk levels. Ground-based measurement locations are indicated with circles coloured by the measured number of days (left half) and corresponding simulated number of days (right half).

#### 4 Summary and conclusions

This study presents a regional-climatic simulation framework based on RegCM4 for investigating the dynamics of emissions and transport of ragweed pollen. The RegCM-pollen modelling system incorporates a pollen emission module coupled to CLM4.5 and a transport module as part of the chemistry transport component of RegCM. Because climate, CLM4.5 and chemistry components are synchronously coupled to the RegCM model, this approach allows dynamical response of pollen ripening, release, and dispersion to key environmental drivers like temperature, photoperiod, soil moisture, precipitation, relative humidity, turbulence, and wind. Through the pollen production link to NPP, other environmental and climate relevant factors as atmospheric CO<sub>2</sub> concentrations are also accounted for. The specific ragweed phenology is parameterized from growth controlled experiment but has to be somehow adjusted to observations for more realism of the flowering season simulations over Europe. Similarly, ragweed spatial distribution is a very poorly constrained parameter which has to be corrected through a

calibration procedure. The calibration is performed considering the decadal mean of pollen counts over all sites. As a result the spatial correlation between the simulated and measured average concentrations over the decade is greatly increased (from 0.23 to 0.98) by the calibration. While the cross validation aimed at evaluating the calibration shows a corresponding correlation of 0.54 and RESM of 21 %, which reflects reasonable error and sensitivity of the calibration. The model measurement correlations based on daily comparison, which are the most relevant for pollen impacts also increase from 0.28 to 0.69. The simulation of daily and interannual variability of pollen concentrations reflect model skills that do not purely rely on the calibration since this one is performed on decadal mean of yearly pollen count.

The RegCM-pollen framework is applied to the European domain for the period 2000–2010. Comparing with the observed flowering season, the model can reproduce starting dates and central dates well, with 68.6 %, 39.2 % of the explained variance and 4.7, 3.9 days of RMSE in starting date and central date, respectively. The pollen season in the main

source regions are reproduced fairly well while in the areas with lower ragweed infestation the deviations are evident. The model in general captures the gross features of the pollen concentrations found in Europe. Statistical measures of NMBF, MFB, and MFE over the domain fall in the range of recommendation for a good performance while NMEF is a bit large with a value of 0.83. The model performs better over the central European source region, where the daily correlations at most stations are above 0.6–0.7 and NMEF lie within 1.0. Performance tends to degrade in France and northern Italy. Still, the values of NMEF for pollen simulation are generally consistent with what is expected from operational air quality models for aerosols for example. Categorical evaluation reveals the model tends to give better predictions for high threshold while giving more false alarms for low threshold. A better performance is also shown over the central European source region at all levels, with correct predictions above 80 % and false alarms within 20 %.

The multi-annual average footprints of ragweed pollen spread risk are produced from calibration simulations. The pollen plume with concentration  $\geq 1$  grains  $\text{m}^{-3}$  can reach seas far away from the European mainland. The risk areas with concentration above 5 grains  $\text{m}^{-3}$  are around the source and on Mediterranean Sea, occupying a total of 29.5 % of domain. While the areas with very strong stress  $\geq 50$  grains  $\text{m}^{-3}$  are confined in narrow source areas. From the seasonal distribution, August in general contributes most to the annual footprint and September shows important levels. The longest risk exposure time occurs on Pannonian Plain at all thresholds. Northern Italy and France also show some considerable exposure times.

The modelling framework presented here allows simultaneous estimation of ragweed pollen risk both for hindcast simulations (including sensitivity studies to different parameters) and for study of potential risk evolution changes under future climate scenarios as illustrated in Hamaoui-Laguel et al. (2015). Still a long list of uncertainties hinders an accurate estimate of the airborne pollen patterns and risk within the presented framework. Caution should also be taken while interpreting the results in areas without a dense observational network and where calibration is weaker. In this regard, challenging research efforts should focus on a better characterization of ragweed spatial distributions and biomass, in addition, a better understanding of phenological process and the dynamic response of release rate to meteorological conditions will help to reduce these uncertainties and improve model performance. An accurate and diverse observation of ragweed phenology is therefore essential to better represent local flowering and there is also a need for experimental observations to better constrain the release model. In parallel, systematic ragweed pollen concentrations should be further developed as part of air quality networks and public access to data should be promoted.

## Data availability

CRUNCEP atmospheric forcing data are available at [http://dods.extra.cea.fr/store/p529viov/cruncep/V5\\_1901\\_2013](http://dods.extra.cea.fr/store/p529viov/cruncep/V5_1901_2013). Data description is available at <http://dods.extra.cea.fr/data/p529viov/cruncep/readme.htm>.

*Acknowledgements.* This research is funded by the European Union's Seventh Framework Programme (FP7/2007–2013) under grant agreements no. 282687 Atopica (<http://cordis.europa.eu/fp7>). We thank the contributors of ragweed distribution data. Pollen observation data are kindly provided by the European Aeroallergen Network, Réseau National de Surveillance Aerobiologique, ARPA-Veneto, ARPA-FVG, Croatian Institute of Public Health, the Department of Environmental Protection and Health Ecology at Institute of Public Health “Andrija Štampar” and Associate-degree college of Velika Gorica. Constructive comments from two anonymous reviewers improved the quality of this paper a lot.

Edited by: S. Fontaine

## References

- Allard, H. A.: Flowering behaviour and natural distribution of the eastern ragweeds (*Ambrosia*) as affected by length of day, *Ecology*, 26, 387–394, 1945.
- Boylan, J. W. and Russell, A. G.: PM and light extinction model performance metrics, goals, and criteria for three-dimensional air quality models, *Atmos. Environ.*, 40, 4946–4959, 2006.
- Bullock, J. M., Chapman, D., Schafer, S., Roy, D., Girardello, M., Haynes, T., Beal, S., Wheeler, B., Dickie, I., Phang, Z., Tinch, R., Čivić, K., Delbaere, B., Jones-Walters, L., Hilbert, A., Schrauwen, A., Prank, M., Sofiev, M., Niemelä, S., Räisänen, P., Lees, B., Skinner, M., Finch, S., and Brough, C.: Assessing and controlling the spread and the effects of common ragweed in Europe, Final Report ENV.B2/ETU/2010/0037, European Commission, 456 pp., 2012.
- Burbach, G. J., Heinzerling, L. M., Röhnelt, C., Bergmann, K.-C., Behrendt, H., and Zuberbier, T.: Ragweed sensitization in Europe – GA(1)LEN study suggests increasing prevalence, *Allergy*, 64, 664–665, 2009.
- Cecchi, L., Morabito, M., Domeneghetti, M. P., Crisci, A., Onorari, M., and Orlandini, S.: Long distance transport of ragweed pollen as a potential cause of allergy in central Italy, *Ann. Allerg. Asthma. Im.*, 96, 86–91, 2006.
- Chapman, D. S., Haynes, T., Beal, S., Essl, F., and Bullock, J. M.: Phenology predicts the native and invasive range limits of common ragweed, *Glob. Change Biol.*, 20, 192–202, 2014.
- Chauvel, B., Dessaint, F., Cardinal-Legrand, C., and Bretagnolle, F.: The historical spread of *Ambrosia artemisiifolia* L. in France from herbarium records, *J. Biogeogr.*, 33, 665–673, 2006.
- Dahl, A., Strandhede, S.-O., and Wihl, J.-A.: Ragweed – An allergy risk in Sweden?, *Aerobiologia*, 15, 293–297, 1999.
- D’Amato, G., Cecchi, L., Bonini, S., Nunes, C., Annesi-Maesano, I., Behrendt, H., Liccardi, G., Popov, T., and Van Cauwenberge, P.: Allergenic pollen and pollen allergy in Europe, *Allergy*, 62, 976–990, 2007.

- Deen, W., Hunt, L. A., and Swanton, C. J.: Photothermal time describes common ragweed (*Ambrosia artemisiifolia* L.) phenological development and growth, *Weed Sci.*, 46, 561–568, 1998a.
- Deen, W., Hunt, T., and Swanton, C. J.: Influence of temperature, photoperiod, and irradiance on the phenological development of common ragweed (*Ambrosia artemisiifolia*), *Weed Sci.*, 46, 555–560, 1998b.
- Deen, W., Swanton, C. J., and Hunt, L. A.: A mechanistic growth and development model of common ragweed, *Weed Sci.*, 49, 723–731, 2001.
- Efstathiou, C., Isukapalli, S., and Georgopoulos, P.: A mechanistic modeling system for estimating large-scale emissions and transport of pollen and co-allergens, *Atmos. Environ.*, 45, 2260–2276, 2011.
- Emanuel, K. A. and Zivkovic-Rothman, M.: Development and evaluation of a convection scheme for use in climate models, *J. Atmos. Sci.*, 56, 1766–1782, 1999.
- Fumanal, B., Chauvel, B., and Bretagnolle, F.: Estimation of pollen and seed production of common ragweed in France, *Ann. Agr. Env. Med.*, 14, 233–236, 2007.
- Galán, C., Smith, M., Thibaudon, M., Frenguelli, G., Oteros, J., Gehrig, R., Berger, U., Clot, B., and Brandao, R.: Pollen monitoring: minimum requirements and reproducibility of analysis, *Aerobiologia*, 30, 385–395, 2014.
- Gallinza, N., Barić, K., Šćepanović, M., Goršić, M., and Ostojić, Z.: Distribution of invasive weed *Ambrosia artemisiifolia* L. in Croatia, *Agriculturae Conspectus Scientificus*, 75, 75–81, 2010.
- García-Mozo, H., Galán, C., Belmonte, J., Bermejo, D., Candau, P., Díaz de la Guardia, C., Elvira, B., Gutiérrez, M., Jato, V., Silva, I., Trigo, M. M., Valencia, R., and Chuine, I.: Predicting the start and peak dates of the Poaceae pollen season in Spain using process-based models, *Agr. Forest Meteorol.*, 149, 256–262, 2009.
- Giorgi, F., Pal, J. S., Bi, X., Sloan, L., Elguindi, N., and Solmon, F.: Introduction to the TAC special issue: The RegCM network, *Theor. Appl. Climatol.*, 86, 1–4, doi:10.1007/s00704-005-0199-z, 2006.
- Giorgi, F., Coppola, E., Solmon, F., Mariotti, L., Sylla, M. B., Bi, X., Elguindi, N., Diro, G. T., Nair, V., Giuliani, G., Turuncoglu, U. U., Cozzini, S., Güttler, I., O'Brien, T. A., Tawfik, A. B., Shalaby, A., Zakey, A. S., Steiner, A. L., Stordal, F., Sloan, L. C., and Brankovic, C.: RegCM4: model description and preliminary tests over multiple CORDEX domains, *Clim. Res.*, 52, 7–29, 2012.
- Grell, G. A.: Prognostic Evaluation of Assumptions Used by Cumulus Parameterizations, *Mon. Weather Rev.*, 121, 764–787, 1993.
- Guenther, A. B., Jiang, X., Heald, C. L., Sakulyanontvittaya, T., Duhl, T., Emmons, L. K., and Wang, X.: The Model of Emissions of Gases and Aerosols from Nature version 2.1 (MEGAN2.1): an extended and updated framework for modeling biogenic emissions, *Geosci. Model Dev.*, 5, 1471–1492, 2012.
- Hamaoui-Laguel, L., Vautard, R., Liu, L., Solmon, F., Viovy, N., Khvorostyanov, D., Essl, F., Chuine, I., Colette, A., Semenov, M. A., Schaffhauser, A., Storkey, J., Thibaudon, M., and Epstein, M. M.: Effects of climate change and seed dispersal on airborne ragweed pollen loads in Europe, *Nature Climate Change*, 5, 766–771, 2015.
- Helbig, N., Vogel, B., Vogel, H., and Fiedler, F.: Numerical modelling of pollen dispersion on the regional scale, *Aerobiologia*, 20, 3–19, 2004.
- Hirst, J. M.: An Automatic Volumetric Spore Trap, *Ann. Appl. Biol.*, 39, 257–265, 1952.
- Holtzlag, A. A. M., De Bruijn, E. I. F., and Pan, H.-L.: A high-resolution air-mass transformation model for short-range weather forecasting, *Mon. Weather Rev.*, 118, 1561–1575, 1990.
- Hurt, G. C., Frolking, S., Fearon, M. G., Moore, B., Shevliakova, E., Malyshev, S., Pacala, S. W., and Houghton, R. A.: The underpinnings of land-use history: three centuries of global gridded land-use transitions, wood-harvest activity, and resulting secondary lands, *Glob. Change Biol.*, 12, 1208–1229, 2006.
- Jäger, S., Mandroli, P., Spieksma, F., Emberlin, J., Hjelmsroos, M., Rantio-Lehtimäki, A., and Al, E.: News, *Aerobiologia*, 11, 69–70, 1995.
- Jato, V., Rodríguez-Rajo, F. J., Alcázar, P., De Nuntiis, P., Galán, C., and Mandrioli, P.: May the definition of pollen season influence aerobiological results?, *Aerobiologia*, 22, 13–25, 2006.
- Karrer, G., Skjøth, C. A., Šikoparija, B., Smith, M., Berger, U., and Essl, F.: Ragweed (*Ambrosia*) pollen source inventory for Austria, *Sci. Total Environ.*, 523, 120–128, 2015.
- Kazinczi, G., Béres, I., Pathy, Z., and Novák, R.: Common ragweed (*Ambrosia artemisiifolia* L.): a review with special regards to the results in Hungary: II. Importance and harmful effect, allergy, habitat, allelopathy and beneficial characteristics, *Herbologia*, 9, 93–117, 2008.
- Martin, M. D., Chamecki, M., and Brush, G. S.: Anthesis synchronization and floral morphology determine diurnal patterns of ragweed pollen dispersal, *Agr. Forest Meteorol.*, 150, 1307–1317, 2010.
- Meleux, F., Solmon, F., and Giorgi, F.: Increase in summer European ozone amounts due to climate change, *Atmos. Environ.*, 41, 7577–7587, 2007.
- Oleson, K. W., Lawrence, D. M., Bonan, G. B., Drewniak, B., Huang, M., Koven, C. D., Levis, S., Li, F., Riley, W. J., Subin, Z. M., Swenson, S. C., Thornton, P. E., Bozbiyik, A., Fisher, R., Heald, C. L., Kluzek, E., Lamarque, J.-F., Lawrence, P. J., Leung, L. R., Lipscomb, W., Muszala, S., Ricciuto, D. M., Sacks, W., Sun, Y., Tang, J., and Yang, Z.-L.: Technical description of version 4.5 of the Community Land Model (CLM), NCAR Technical Note NCAR/TN-503+STR, National Center for Atmospheric Research, Boulder, Colorado, 434 pp., 2013.
- Oswalt, M. L. and Marshall, G. D.: Ragweed as an example of worldwide allergen expansion, *Allergy Asthma Clin. Immunol.*, 4, 130–135, 2008.
- Pal, J. S., Small, E. E., and Eltahir, E. A. B.: Simulation of regional-scale water and energy budgets: Representation of subgrid cloud and precipitation processes within RegCM, *J. Geophys. Res. Atmos.*, 105, 29579–29594, 2000.
- Pal, J. S., Giorgi, F., Bi, X., Elguindi, N., Solmon, F., Rauscher, S. A., Gao, X., Francisco, R., Zakey, A., Winter, J., Ashfaq, M., Syed, F. S., Sloan, L. C., Bell, J. L., Diffenbaugh, N. S., Karmacharya, J., Konaré, A., Martinez, D., da Rocha, R. P., and Steiner, A. L.: Regional climate modeling for the developing world: the ICTP RegCM3 and RegCM3, *B. Am. Meteorol. Soc.*, 88, 1395–1409, 2007.
- Payne, W. W.: The morphology of the inflorescence of ragweeds (*Ambrosia-Franseria*: Compositae), *Am. J. Bot.*, 50, 872–880, 1963.
- Pinke, G., Karácsony, P., Czúcz, B., and Botta-Dukat, Z.: Environmental and land-use variables determining the abundance of Am-

- brosia artemisiifolia in arable fields in Hungary, *Preslia*, 83, 219–235, 2011.
- Prank, M., Chapman, D. S., Bullock, J. M., Belmonte, J., Berger, U., Dahl, A., Jager, S., Kovtunen, I., Magyar, D., Niemela, S., Rantio-Lehtimäki, A., Rodinkova, V., Sauliene, I., Severova, E., Sikoparija, B., and Sofiev, M.: An operational model for forecasting ragweed pollen release and dispersion in Europe, *Agr. Forest Meteorol.*, 182, 43–53, 2013.
- Rogers, C. A., Wayne, P. M., Macklin, E. A., Muilenberg, M. L., Wagner, C. J., Epstein, P. R., and Bazzaz, F. A.: Interaction of the onset of spring and elevated atmospheric CO<sub>2</sub> on ragweed (*Ambrosia artemisiifolia* L.) pollen production, *Environ. Health Persp.*, 114, 865–869, 2006.
- Shalaby, A. K., Zakey, A. S., Tawfik, A. B., Solmon, F., Giorgi, F., Stordal, F., Sillman, S., Zaveri, R. A., and Steiner, A. L.: Implementation and evaluation of online gas-phase chemistry within a regional climate model (RegCM-CHEM4), *Geosci. Model Dev.*, 5, 741–760, doi:10.5194/gmd-5-741-2012, 2012.
- Shrestha, A., Roman, E. S., Thomas, A. G., and Swanton, C. J.: Modeling germination and shoot-radicle elongation of *Ambrosia artemisiifolia*, *Weed Sci.*, 47, 557–562, 1999.
- Šikoparija, B., Skjøth, C. A., Radišić, P., Stjepanović, B., Hrga, I., Apatini, D., Martinez, D., Páldy, A., Ianovici, N., and Smith, M.: Aerobiology data used for producing inventories of invasive species, in: Proceedings of the international symposium on current trends in plant protection, Belgrade, Serbi, 8 September 2012, 7–14, 2012.
- Šikoparija, B., Skjøth, C. A., Kübler, K. A., Dahl, A., Sommer, J., Grewling, L., Radišić, P., and Smith, M.: A mechanism for long distance transport of *Ambrosia* pollen from the Pannonian Plain, *Agr. Forest Meteorol.*, 180, 112–117, 2013.
- Simard, M. J. and Benoit, D. L.: Effect of repetitive mowing on common ragweed (*Ambrosia artemisiifolia* L.) pollen and seed production, *Ann. Agr. Env. Med.*, 18, 55–62, 2011.
- Simard, M. J. and Benoit, D. L.: Potential pollen and seed production from early- and late-emerging common ragweed in corn and soybean, *Weed Technol.*, 26, 510–516, 2012.
- Skjøth, C. A.: Integrating measurements, phenological models and atmospheric models in aerobiology, Ph.D. thesis, Copenhagen University and National Environmental Research Institute, Denmark, 123 pp., 2009.
- Skjøth, C. A., Smith, M., Šikoparija, B., Stach, A., Myszkowska, D., Kasprzyk, I., Radišić, P., Stjepanović, B., Hrga, I., Apatini, D., Magyar, D., Páldy, A., and Ianovici, N.: A method for producing airborne pollen source inventories: An example of *Ambrosia* (ragweed) on the Pannonian Plain, *Agr. Forest Meteorol.*, 150, 1203–1210, 2010.
- Smith, M., Skjøth, C. A., Myszkowska, D., Uruska, A., Puc, M., Stach, A., Balwierz, Z., Chlopek, K., Piotrowska, K., Kasprzyk, I., and Brandt, J.: Long-range transport of *Ambrosia* pollen to Poland, *Agr. Forest Meteorol.*, 148, 1402–1411, 2008.
- Smith, M., Cecchi, L., Skjøth, C. A., Karrer, G., and Šikoparija, B.: Common ragweed: A threat to environmental health in Europe, *Environ. Int.*, 61, 115–126, 2013.
- Sofiev, M., Siljamo, P., Ranta, H., and Rantio-Lehtimäki, A.: Towards numerical forecasting of long-range air transport of birch pollen: theoretical considerations and a feasibility study, *Int. J. Biometeorol.*, 50, 392–402, 2006.
- Sofiev, M., Siljamo, P., Ranta, H., Linkosalo, T., Jaeger, S., Rasmussen, A., Rantio-Lehtimäki, A., Severova, E., and Kukkonen, J.: A numerical model of birch pollen emission and dispersion in the atmosphere, Description of the emission module, *Int. J. Biometeorol.*, 57, 45–58, 2013.
- Sofiev, M., Berger, U., Prank, M., Vira, J., Arteta, J., Belmonte, J., Bergmann, K. C., Chéroux, F., Elbern, H., Friese, E., Galan, C., Gehrig, R., Khvorostyanov, D., Kranenburg, R., Kumar, U., Maréchal, V., Meleux, F., Menut, L., Pessi, A. M., Robertson, L., Rittenberga, O., Rodinkova, V., Saarto, A., Segers, A., Severova, E., Sauliene, I., Siljamo, P., Steensen, B. M., Teinmaa, E., Thibaudon, M., and Peuch, V. H.: MACC regional multi-model ensemble simulations of birch pollen dispersion in Europe, *Atmos. Chem. Phys.*, 15, 8115–8130, 10.5194/acp-15-8115-2015, 2015.
- Solmon, F., Giorgi, F., and Liousse, C.: Aerosol modelling for regional climate studies: application to anthropogenic particles and evaluation over a European/African domain, *Tellus B*, 58, 51–72, 2006.
- Solmon, F., Elguindi, N., and Mallet, M.: Radiative and climatic effects of dust over West Africa, as simulated by a regional climate model, *Clim. Res.*, 52, 97–113, 2012.
- Stach, A., Smith, M., Skjøth, C. A., and Brandt, J.: Examining *Ambrosia* pollen episodes at Poznan (Poland) using back-trajectory analysis, *Int. J. Biometeorol.*, 51, 275–286, 2007.
- Storkey, J., Stratonovitch, P., Chapman, D. S., Vidotto, F., and Semenov, M. A.: A process-based approach to predicting the effect of climate change on the distribution of an invasive allergenic plant in Europe, *Plos One*, 9, e88156, doi:10.1371/journal.pone.0088156, 2014.
- Tamarcaz, P., Lambelet, C., Clot, B., Keimer, C., and Hauser, C.: Ragweed (*Ambrosia*) progression and its health risks: will Switzerland resist this invasion?, *Swiss Med. Wkly.*, 135, 538–548, 2005.
- Thibaudon, M., Šikoparija, B., Oliver, G., Smith, M., and Skjøth, C. A.: Ragweed pollen source inventory for France – The second largest centre of *Ambrosia* in Europe, *Atmos. Environ.*, 83, 62–71, 2014.
- Thornton, P. E., Law, B. E., Gholz, H. L., Clark, K. L., Falge, E., Ellsworth, D. S., Golstein, A. H., Monson, R. K., Hollinger, D., Falk, M., Chen, J., and Sparks, J. P.: Modeling and measuring the effects of disturbance history and climate on carbon and water budgets in evergreen needleleaf forests, *Agr. Forest Meteorol.*, 113, 185–222, 2002.
- Thornton, P. E., Lamarque, J. F., Rosenbloom, N. A., and Mahowald, N. M.: Influence of carbon-nitrogen cycle coupling on land model response to CO<sub>2</sub> fertilization and climate variability, *Global Biogeochem. Cy.*, 21, GB4018, doi:10.1029/2006gb002868, 2007.
- Tummon, F., Solmon, F., Liousse, C., and Tadmoss, M.: Simulation of the direct and semidirect aerosol effects on the southern Africa regional climate during the biomass burning season, *J. Geophys. Res.-Atmos.*, 115, D19206, doi:10.1029/2009JD013738, 2010.
- Viovy, N.: CRUNCEP dataset, Description available at: <http://dods.extra.cea.fr/data/p529viov/cruncep/readme.htm>, Data available at: [http://dods.extra.cea.fr/store/p529viov/cruncep/V5\\_1901\\_2013](http://dods.extra.cea.fr/store/p529viov/cruncep/V5_1901_2013), 2011.
- Willemsen, R. W.: Effect of stratification temperature and germination temperature on germination and induction of secondary

- dormancy in common ragweed seeds, *Am. J. Bot.*, 62, 1–5, doi:10.2307/2442073, 1975.
- Yu, S. C., Eder, B., Dennis, R., Chu, S.-H., and Schwartz, S. E.: New unbiased symmetric metrics for evaluation of air quality models, *Atmos. Sci. Lett.*, 7, 26–34, 2006.
- Zakey, A. S., Solmon, F., and Giorgi, F.: Implementation and testing of a desert dust module in a regional climate model, *Atmos. Chem. Phys.*, 6, 4687–4704, doi:10.5194/acp-6-4687-2006, 2006.
- Zhang, R., Duhl, T., Salam, M. T., House, J. M., Flagan, R. C., Avol, E. L., Gilliland, F. D., Guenther, A., Chung, S. H., Lamb, B. K., and VanReken, T. M.: Development of a regional-scale pollen emission and transport modeling framework for investigating the impact of climate change on allergic airway disease, *Biogeosciences*, 11, 1461–1478, doi:10.5194/bg-11-1461-2014, 2014.
- Zhang, Y., Liu, P., Queen, A., Misenis, C., Pun, B., Seigneur, C., and Wu, S.-Y.: A comprehensive performance evaluation of MM5-CMAQ for the Summer 1999 Southern Oxidants Study episode – Part II: Gas and aerosol predictions, *Atmos. Environ.*, 40, 4839–4855, 2006.
- Zhang, Y., Bocquet, M., Mallet, V., Seigneur, C., and Baklanov, A.: Real-time air quality forecasting, Part I: History, techniques, and current status, *Atmos. Environ.*, 60, 632–655, 2012.
- Zink, K., Vogel, H., Vogel, B., Magyar, D., and Kottmeier, C.: Modeling the dispersion of *Ambrosia artemisiifolia* L. pollen with the model system COSMO-ART, *Int. J. Biometeorol.*, 56, 669–680, 2012.
- Zink, K., Pauling, A., Rotach, M. W., Vogel, H., Kaufmann, P., and Clot, B.: EMPOL 1.0: a new parameterization of pollen emission in numerical weather prediction models, *Geosci. Model Dev.*, 6, 1961–1975, 2013.